DOI: 10.18721/JPM.12201
УДК 519.6:533.6.011

NUMERICAL SOLUTION OF A 3D PROBLEM ON A SUPERSONIC VISCOUS GAS FLOW PAST A PLATE-CYLINDRICAL BODY JUNCTION AT M 2.95

E.V. Kolesnik, E.M. Smirnov, A.A. Smirnovsky

Peter the Great St. Petersburg Polytechnic University, St. Petersburg, Russian Federation

In the paper, results of numerical simulation of a shock-wave pattern and vortex structures forming in supersonic flow past an adjacent-to-plate elongate cylindrical body, which penetrates the developing flat-plate boundary layer, have been presented. The laminar flow regime at Mach number 2.95 was considered, Reynolds number was taken 4000. The solutions were obtained using two schemes for convective flux (HLL and AUSM). Comparison of the flow fields computed with the mentioned schemes of the first and second orders of accuracy were conducted. Solution mesh sensitivity issues were discussed.

Keywords: high-speed flow, viscous-inviscid interaction, numerical simulation, AUSM and HLL schemes

Citation: Kolesnik E.V., Smirnov E.M., Smirnovsky A.A., Numerical solution of a 3D problem on a supersonic viscous gas flow past a plate-cylindrical body junction at M 2.95, St. Petersburg Polytechnical State University Journal. Physics and Mathematics. 12 (2) (2019) 7–22. DOI: 10.18721/JPM.12201

ЧИСЛЕННОЕ РЕШЕНИЕ ТРЕХМЕРНОЙ ЗАДАЧИ ОБТЕКАНИЯ УСТАНОВЛЕННОГО НА ПЛАСТИНЕ ЦИЛИНДРИЧЕСКОГО ТЕЛА СВЕРХЗВУКОВЫМ ПОТОКОМ ВЯЗКОГО ГАЗА ПРИ M = 2,95

Е.В. Колесник, Е.М. Смирнов, А.А. Смирновский

Санкт-Петербургский политехнический университет Петра Великого,
Санкт-Петербург, Российская Федерация

Представлены результаты численного моделирования ударно-волновых и вихревых структур, которые формируются при обтекании сверхзвуковым потоком удлиненного цилиндрического тела, которое примыкает к пластине и пронизывает развивающийся на пластине пограничный слой. Рассмотрен ламинарный режим течения при числе Маха набегающего потока, равном 2,95, и числе Рейнольдса, равном 4000. Решения получены с использованием двух схем для расчета конвективных потоков (HLL и AUSM). Проведено сравнение полей течения, рассчитанных с применением указанных численных схем первого и второго порядков точности. Обсуждаются вопросы сходимости численного решения по сетке.

Ключевые слова: высокоскоростное течение, вязко-невязкое взаимодействие, численное моделирование, схема AUSM, схема HLL

Ссылка при цитировании: Колесник Е.В., Смирнов Е.М., Смирновский А.А. Численное решение трехмерной задачи обтекания установленного на пластине цилиндрического тела сверхзвуковым потоком вязкого газа при M = 2,95// Научно-технические ведомости СПбГПУ. Физико-математические науки. 2019. Т. 12. № 2. С. 7–22. DOI: 10.18721/JPM.12201

Introduction

Practical problems of the aerospace industry and turbomachinery often involve studies on the structure of subsonic and supersonic flows around structural elements fixed on the streamlined surface. This includes, in particular, design of connections between wings, fuselage, tail and other elements, and optimization of interaction of supersonic flow with injected gas jets used in control elements.

Keen interest in this type of problems was instigated by development of supersonic and hypersonic aircraft construction started in the mid-20th century. One of the challenging tasks here is three-dimensional flow with a complex shock-wave structure, a wide separation region and a system of horseshoe-shaped vortices that takes place in supersonic viscous gas flow around the junction of a blunt body with a plate. In other words, the effects of viscous-inviscid interaction in supersonic flow of viscous gas can be clearly observed in this problem.

On the whole, sufficient detailed information has been ~~collected~~ obtained in recent years for the case of the interaction of a separating boundary layer with a bow shock. Reviews of literature on this topic can be found, for example, in [1, 2].

A case of a separation region forming in front of the body in subsonic flow is also of interest. For instance, this applies to problems of turbomachine engineering, where understanding the complex vortex structure of the flow near the leading edge of the blade is important for taking into account the heat transfer patterns in the region of the blade/endwall junction in ~~disks~~ vanes of high-temperature gas turbines. Many studies, both experimental and computational, have been dedicated to studying the flow structure in subsonic regime (see, for example, [3–6]).

The subject of this study is one of the model problems simulating the complex structure of three-dimensional flow. We have considered supersonic flow around an elongated cylindrical body mounted on a plate along which the boundary layer evolves (Fig. 1). A fairly large number of experimental works [7–13] addressed this problem. Some of the earliest studies of the flow structure in this configuration [7–9] revealed that local supersonic regions and bow shocks, inducing a secondary separation region inside the main zone, evolve in front of the cylindrical body.

One of the most important characteristic for high-speed aircraft is the intensity of heat transfer in front of the streamlined body; studies indicate strong intensification of heat transfer in this region. In particular, a recently published paper [13] considered local heat transfer on a plate with flow around a cylindrical body at a Mach number of 5.

It is rather problematic to experimentally obtain sufficient data on the detailed structure of three-dimensional supersonic flow in the entire region where it develops. For this reason, it would be of great interest to be able to predict the flow structure in the given model configuration based on computational fluid dynamics, providing high quality of resolution for the regions with viscous-inviscid interaction. The first studies on numerical simulation of laminar and turbulent flows in the given configuration [14, 15] used computational meshes that could not provide sufficient resolution of all flow features. A relatively recent work [16], detailing extensive study (both experimental and numerical) of the flow around a blunt body at Mach number M = 6.7 was performed, established, for example, that a sufficiently accurate resolution of the flow structure is obtained with a mesh size of about 15 million cells.

Numerical simulation of supersonic flow under given conditions may be complicated by the so-called carbuncle instability [17, 18], which leads to strong distortion of bow shock in the numerical solution. This instability may occur when using several well-known numerical schemes; different approaches (in particular,

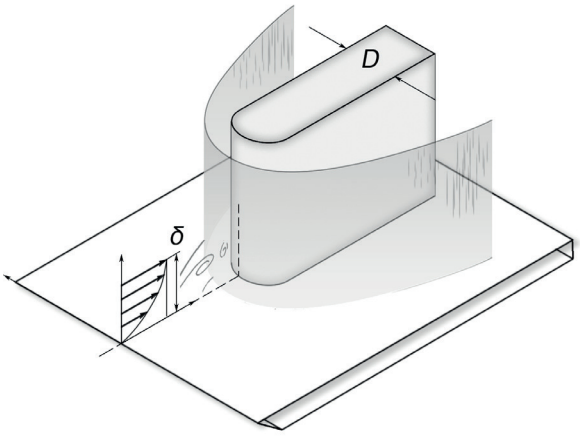

Fig. 1. Schematic representation of problem statement:
viscous gas flow around elongated cylindrical body with diameter D of blunt part, mounted on plate; boundary layer develops along the plate (δ is the thickness of this layer)

hybrid schemes [18, 16] and introduction of additional artificial viscosity [19]) have been devised to suppress it. There are also schemes where the carbuncle instability is usually not observed. These include the Harten–Lax–van Leer (HLL) scheme [20], which is characterized by high dissipativity, and a family of schemes based on s flux vector splitting, proposed by Liou and Steffen (Advection Upstream Splitting Method (AUSM)) [21], which many authors have found to be stable to non-physical oscillations on the bow shock.

The majority of published works on numerical solution to the problem of high-speed flow of viscous gas around a blunt body mounted on a plate considered a case of hypersonic flow. However, little attention has been paid in literature to flows with moderate free-stream Mach numbers and the quality of numerical prediction of the effects of viscous-inviscid interaction.

In this paper, we present the results of a numerical solution to the problem of flow past an elongated blunt body mounted on a plate, with the free-stream Mach number equal to 2.95, and the Reynolds number based on the diameter of the blunt part equal to 4000. A moderate Reynolds number, ensuring laminar flow in the given region, was chosen because we focused on obtaining an accurate, almost grid-converged solution, with detailed resolution of both the complex structure of the flow in the viscous separation region with a system of horseshoe-shaped vortices, and the gas-dynamic structure characterized by detached shock and a system of oblique compression waves generated by flow around the separation region.

Numerical solutions were obtained by two schemes, HLL and AUSM; both of them allowed to avoid the carbuncle instability. Additionally, we have carried out comparative analysis of the solutions.

Numerical method for solving the problem

General formulation. The following numerical solutions for viscous gas flow were obtained using the finite volume method (FVM), based on integral formulation of the laws of conservation of mass, momentum and energy, as applied to computational cell (control volume):

$$\int_{\Omega} \frac{\partial \mathbf{w}}{\partial \tau} d\Omega + \sum_{M} \int_{S_m} \mathbf{F}^{\Sigma} dS = 0, \qquad (1)$$

where Ω is the control volume; M is the number of its faces; S_m is the area of the current face, m $= \overline{1,M}$, $\mathbf{F}^{\Sigma}$ is the vector of the fluxes on the face of the control volume; w = [ρ,ρu,ρv,ρw,ρE] is the vector of conservative variables ($u \equiv u_1$, $v \equiv u_2$, $w \equiv u_3$ are the components of the velocity vector **V** in the Cartesian coordinate system; E is the total energy; ρ is the density).

The vector $\mathbf{F}^{\Sigma}$ is the sum of vectors of inviscid and viscous fluxes $\mathbf{F}^{\Sigma} = \mathbf{F} + \mathbf{F}^{visc}$, defined by the expressions:

$$\mathbf{F} = \begin{bmatrix} \rho \mathbf{V} \cdot \mathbf{n} \\ \rho \mathbf{V} \cdot \mathbf{n} u + p \mathbf{n} \cdot \mathbf{i} \\ \rho \mathbf{V} \cdot \mathbf{n} v + p \mathbf{n} \cdot \mathbf{j} \\ \rho \mathbf{V} \cdot \mathbf{n} w + p \mathbf{n} \cdot \mathbf{k} \\ \rho \mathbf{V} \cdot \mathbf{n} H \end{bmatrix}, \qquad (2)$$

$$\mathbf{F}^{visc} = \begin{bmatrix} 0 \\ \mathbf{n} \cdot \boldsymbol{\tau} \cdot \mathbf{i} \\ \mathbf{n} \cdot \boldsymbol{\tau} \cdot \mathbf{j} \\ \mathbf{n} \cdot \boldsymbol{\tau} \cdot \mathbf{k} \\ \mathbf{n} \cdot (\boldsymbol{\tau} \cdot \mathbf{V} + \mathbf{q}) \end{bmatrix}, \qquad (2)$$

where p is the pressure; H is the total enthalpy; **n** is the normal to the face; **i**, **j**, **k** are the unit vectors of the Cartesian coordinate system ($x \equiv x_1$, $y \equiv x_2$, $z \equiv x_3$).

The components of the viscous stress tensor **τ** and the heat flux density vector **q** are written as

$$\tau_{ij} = \mu \left[\left(\frac{\partial u_i}{\partial x_j} + \frac{\partial u_j}{\partial x_i} \right) - (2/3) \frac{\partial u_k}{\partial x_k} \delta_{ij} \right], \qquad (3)$$

$$q_j = -\lambda \left(\partial T / \partial x_j \right), \qquad (4)$$

where T is the temperature; μ is the dynamic viscosity of the gas whose dependence on temperature is determined by the Sutherland formula; λ is the thermal conductivity of the gas.

The total energy and enthalpy are determined by the expressions:

$$E = c_v T + V^2/2, \; H = c_p T + V^2/2,$$

where cv, cp are the specific heat capacities at constant volume and constant pressure,

respectively; they are assumed to be constant.

Pressure p, density ρ and internal energy e are related by the equation of state of a perfect gas:

$$p = (\gamma - 1)\rho e,$$

where γ is the adiabatic index ($\gamma = cp/cv$).

Simulation schemes for convective flows. The method for inviscid fluxes $\mathbf{F}$ approximation is especially important in simulation of supersonic flows. The approximation scheme should provide sufficiently accurate resolution of gas dynamic discontinuities with a small number of internal points in the absence of flow field oscillations near the discontinuities. The methods with desired behavior, which are based on characteristic properties of the system of equations, have gained great popularity over the past decades [22]. These include flux vector splitting schemes (for example, the Steger–Warming splitting scheme, the AUSM method), and schemes based on the Riemann solver for the discontinuity problem (for example, Godunov, Roe, HLL and HLLC schemes). Below, we consider ~~in detail~~ only the AUSM and HLL schemes selected for our computations.

Parameters for the "left" and "right" sides of a given face are widely used in flux computations (denoted by subscripts L and R below). If values from the centers of adjacent cells are used as such parameters, the numerical method is of the first order of accuracy. Special methods for evaluating the parameters to the left and right of the face (briefly discussed below) can be used to implement schemes with a higher order of accuracy.

AUSM scheme [21]. The flux vector $\mathbf{F}$ is represented as the sum of $\mathbf{F}^{(c)}$ (convective component) and $\mathbf{F}^{(p)}$ (component related to pressure):

$$\mathbf{F} = \begin{bmatrix} \rho\mathbf{V}\cdot\mathbf{n} \\ \rho\mathbf{V}\cdot\mathbf{n}u + p\mathbf{n}\cdot\mathbf{i} \\ \rho\mathbf{V}\cdot\mathbf{n}v + p\mathbf{n}\cdot\mathbf{j} \\ \rho\mathbf{V}\cdot\mathbf{n}w + p\mathbf{n}\cdot\mathbf{k} \\ \rho\mathbf{V}\cdot\mathbf{n}H \end{bmatrix} = \begin{bmatrix} \rho\mathbf{V}\cdot\mathbf{n} \\ \rho\mathbf{V}\cdot\mathbf{n}u \\ \rho\mathbf{V}\cdot\mathbf{n}v \\ \rho\mathbf{V}\cdot\mathbf{n}w \\ \rho\mathbf{V}\cdot\mathbf{n}H \end{bmatrix} + \begin{bmatrix} 0 \\ p\mathbf{n}\cdot\mathbf{i} \\ p\mathbf{n}\cdot\mathbf{j} \\ p\mathbf{n}\cdot\mathbf{k} \\ 0 \end{bmatrix} = \mathbf{F}^{(c)} + \mathbf{F}^{(p)}. \quad (5)$$

Accordingly, $\mathbf{F}_f$ (numerical flux on the face) is also found as the sum:

$$\mathbf{F}_f = \mathbf{F}_f^{(c)} + \mathbf{F}_f^{(p)}. \quad (6)$$

A specific splitting method is used for each of the components.

The convective flux $\mathbf{F}^{(c)}$ is expressed in terms of the Mach number M constructed from the normal velocity component:

$$\mathrm{M} = \mathbf{V}\cdot\mathbf{n}/a,$$

where $a = \sqrt{\gamma RT}$ is the speed of sound (R is the gas constant):

$$\mathbf{F}^{(c)} = \mathrm{M}\begin{bmatrix} \rho a \\ \rho a u \\ \rho a v \\ \rho a w \\ \rho a H \end{bmatrix} \equiv \mathrm{M}\hat{\mathbf{F}}^{(c)}. \quad (7)$$

Splitting of the convective flux is based on the sign of the Mach number at the face M_f in the following manner:

$$\mathbf{F}_f^{(c)} = \begin{cases} \mathrm{M}_f\left[\hat{\mathbf{F}}^{(C)}\right]_L, & \mathrm{M}_f \geq 0, \\ \mathrm{M}_f\left[\hat{\mathbf{F}}^{(C)}\right]_R, & \mathrm{M}_f < 0. \end{cases} \quad (8)$$

The Mach number at the face is found as the sum of the positive and negative components:

$$\mathrm{M}_f = \mathrm{M}_L^+ + \mathrm{M}_R^-,$$

where the splitting into components is carried out using the following relationship:

$$\mathrm{M}_{L/R}^{\pm} = \begin{cases} \pm\frac{1}{4}(\mathrm{M}_{L/R} \pm 1)^2, & |\mathrm{M}_{L/R}| \leq 1; \\ \frac{1}{2}(\mathrm{M}_{L/R} \pm |\mathrm{M}_{L/R}|), & |\mathrm{M}_{L/R}| > 1. \end{cases} \quad (9)$$

The component of the flux related to pressure is defined as

$$\mathbf{F}_f^{(\mathrm{p})} = \left(p_L^+ + p_R^-\right)\begin{bmatrix} 0 \\ \mathbf{n}\cdot\mathbf{i} \\ \mathbf{n}\cdot\mathbf{j} \\ \mathbf{n}\cdot\mathbf{k} \\ 0 \end{bmatrix}, \quad (10)$$

where the splitting of pressure into the positive and the negative component is also carried out depending on the Mach number:

$$p^{\pm}_{L/R} = \begin{cases} \pm\dfrac{p_{L/R}}{4}(\mathrm{M}_{L/R} \pm 1)^2(2 \mp \mathrm{M}_{L/R}), \\ |\mathrm{M}_{L/R}| \le 1; \\ \dfrac{p_{L/R}}{2}\dfrac{(\mathrm{M}_{L/R} \pm |\mathrm{M}_{L/R}|)}{\mathrm{M}_{L/R}}, \\ |\mathrm{M}_{L/R}| > 1. \end{cases} \quad (11)$$

HLL scheme [20]. The scheme is based on the approximate Riemann solver for the discontinuity problem. It is assumed that the solution consists of two main discontinuities describing the propagation only of strong waves such as shock waves; other waves, such as contact or tangential discontinuities, are not taken into account.

The velocities of the main discontinuities (characteristics) S_L and S_R comprising solution are defined by the following expressions [23]:

$$S_L = \min\left(\mathbf{V}_L \cdot \mathbf{n} - a_L, \tilde{\mathbf{V}} \cdot \mathbf{n} - \tilde{a}\right), \quad (12)$$

$$S_R = \min\left(\mathbf{V}_R \cdot \mathbf{n} + a_R, \tilde{\mathbf{V}} \cdot \mathbf{n} + \tilde{a}\right), \quad (13)$$

where a_L and a_R are the speeds of sound computed by the parameters on the left and right sides of the face; the quantities e and $\tilde{\mathbf{V}}$ are the variables computed for the current face by means of Roe averaging [24].

According to the approximate Riemann solver [20], the characteristics of S_L and S_R are separated from each other by three regions with constant gas parameters on the x–t diagram: two regions with undisturbed gas parameters "left" and "right" from the face, and the third region between them.

Numerical flux on the face depends on the configuration corresponding to the current face:

$$\mathbf{F}_f = \begin{cases} \mathbf{F}_L, \ 0 \le S_L; \\ \mathbf{F}^*, \ S_L \le 0 \le S_R; \\ \mathbf{F}_R, \ 0 \ge S_R, \end{cases} \quad (14)$$

where the flux $\mathbf{F}^*$ is found by the formula

$$\mathbf{F}^* = \frac{S_R\mathbf{F}_L - S_L\mathbf{F}_R + S_L S_R(\mathbf{w}_R - \mathbf{w}_L)}{S_R - S_L}. \quad (15)$$

Increasing the order of accuracy. The order of accuracy of a numerical scheme can be increased with a technique for quasi-monotonic interpolation of mesh solutions: the MUSCL approach (Monotonic Upstream-Centered Scheme for Conservation Laws) [25], which is used for piecewise polynomial reconstruction of the solution in each control volume and

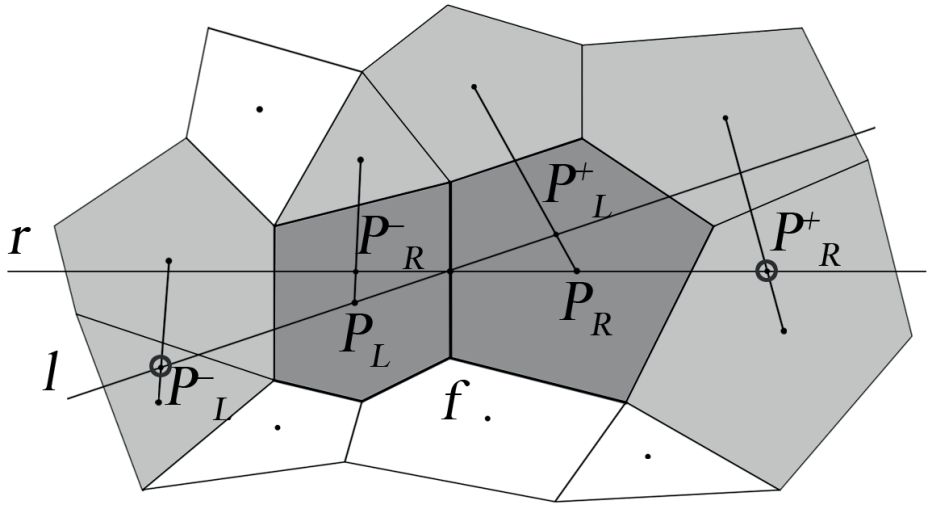

Fig. 2. Scheme for constructing algorithm for quasi-one-dimensional computations in two-dimensional case;
left and right cells adjacent to the given face f are highlighted in dark gray, all stencil cells used for determining the values at additional points (notations are given for them) are highlighted in light gray;
r, l are direct reconstructions for face f

for reconstruction of the values on the face with increased accuracy. Total Variation Diminishing schemes (TVD) are applied to obtain monotonous solutions in computations by second-order accuracy schemes [26]. This approach can be generalized to the case of unstructured meshes by applying quasi-one-dimensional computations with some suitable direction (similar to the coordinate direction initially present in structured meshes) selected locally for each face. In other words, aside from the values of the variables in the centers of the cells located on both sides of the face, at least two more virtual points to the left and right of the center points (points P_L^+, P_L^-, P_R^+ and P_L^- in Fig. 2) are required, in which the values of variables can be reconstructed in some way.

The numerical solutions given below were obtained using the approach proposed in [27] and described in detail in [28]. Two straight lines (reconstruction beam) are drawn through the center of each face f and through the centers of the cells adjacent to the face (direct reconstructions are l and r in Fig. 2); two additional points are taken on each of these straight lines, with the values of the variables in these points ~~found~~ evaluated by interpolation based on the known values of the variables in certain neighboring centers of the cells ("interpolating triples").

Such cells are found by the following algorithm [28]: first, a set N_1 is established, including all first-level neighbors for the current cell, i.e., the set of cells that have at least one common node with the current cell, excluding the cell itself. Next, all cells from the set N_1 are sorted by ascending cosine of the angle between the reconstruction beam emanating from the center of the current cell and the vector of direction to the center of the cell from this set. Next, an iterative search of the cell triplets is performed in ascending order of the sum of the indices of these cells in the sorted array and the first of the "interpolating triplets" found is used. By interpolating triplet we mean a triplet of cells whose centers form a triangle and the straight line of reconstruction intersects it.After the values at additional points have been computed, the values on the left and right sides of the face are found in accordance with one-sided linear extrapolation:

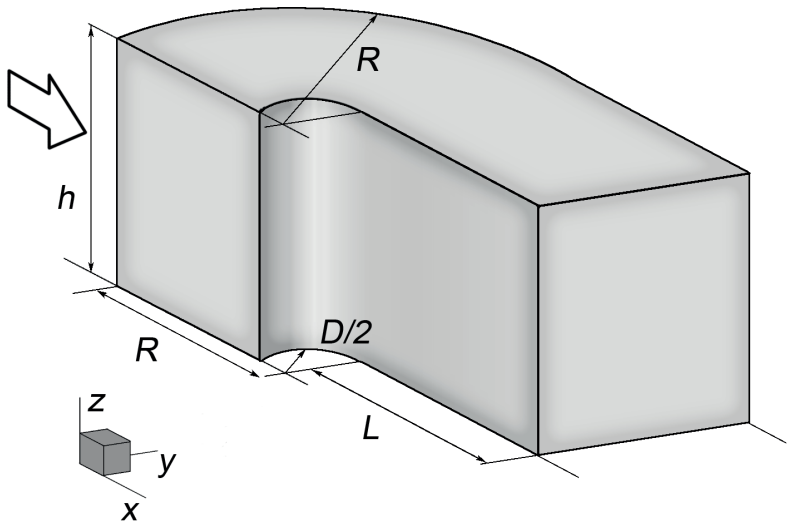

Fig. 3. Computational domain for problem of supersonic flow around elongated cylindrical body (see Fig. 1).
The figure shows the geometrical parameters: D is the diameter of the blunt part of the body, R, L, h are the dimensions of the computational domain, the arrow indicates the direction of the flux

$$u_L^f = u_L + \psi_L \left(u_L - u_L^-\right)/2, \qquad (16)$$

$$u_R^f = u_R - \psi_R \left(u_R^+ - u_R\right)/2, \qquad (17)$$

where u is any of the reconstructed variables; $\psi(r)$ is the limiter introduced to control oscillations and computed as a function of the ratio of two differences:

$$\psi_L = \psi_L \left(\left(u_L^+ - u_L\right)/\left(u_L - u_L^-\right)\right), \qquad (18)$$

$$\psi_R = \psi_R \left(\left(u_R^- - u_R\right)/\left(u_R - u_R^+\right)\right). \qquad (19)$$

We used Van Albada's TVD-limiter [29] as the function ψ in these computations.

Problem statement and computational tools

Fig. 3 shows the computational domain for the given problem of supersonic flow past an elongated cylindrical body mounted on an adiabatic plate along which a laminar boundary layer evolves. The flow is assumed to be symmetrical, so the computational domain covers only half of the initial configuration. The dimensions of the region are: $R = 15D$, $h = 10D$, $L = 8D$, where D is the diameter of the blunt part of the body, also assumed to be adiabatic.

The problem is governed by the following set of dimensionless parameters: the free-stream Mach number M, the Reynolds number Re_D, the Prandtl number Pr, the adiabatic index γ and the ratio D/δ of the body's diameter to the thickness of the incoming boundary layer. The numerical solutions in this study were obtained for M = 2.95, $\mathrm{Re}_D = 4000$, Pr = 0.71, $\gamma = 1.4$, $D/\delta_{95\%} = 1$. Velocity and temperature profiles for the boundary layer of a given thickness $\delta_{95\%}$ were prescribed at the inlet boundary of the computational domain.

We have implemented the above-described numerical method in combination with the implicit scheme in "increments" as one of the options of the finite-volume unstructured ~~program~~ code SINF/Flag-S, which is under development at the Hydroaerodynamics, Combustion and Heat Transfer Department of Peter the Great St. Petersburg Polytechnic University.

The resources of the Polytechnic Supercomputer Center (www.scc.spbstu.ru) were used for computations.

Computation results and discussion

Flow structure. The numerical solution obtained by the AUSM scheme on the most refined of the meshes used is shown in Figs. 4–6 (the issues of grid-converged solution are discussed below). In general, the structure of the computed flow field is similar to that described

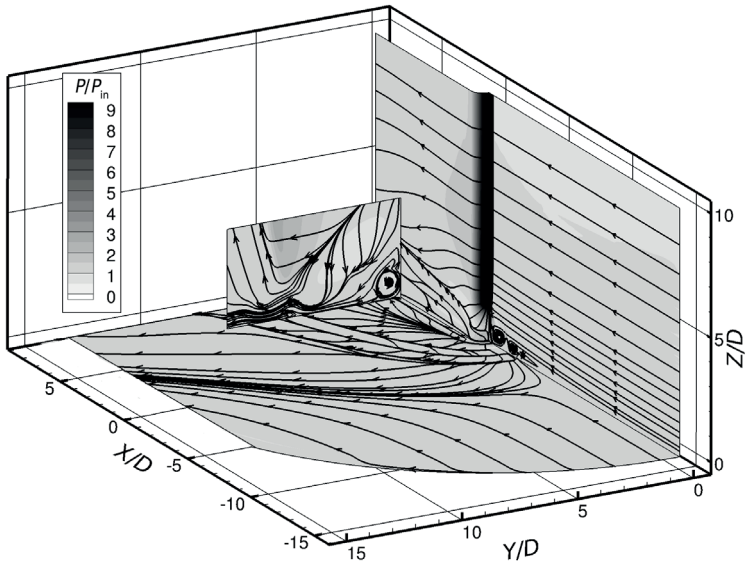

Fig. 4. Surface streamlines and flow structure in axial (*XZ* plane) and transverse (*XY*) cross-sections of flow. Pressure distributions in these cross sections and on the surface of the streamlined body are also shown

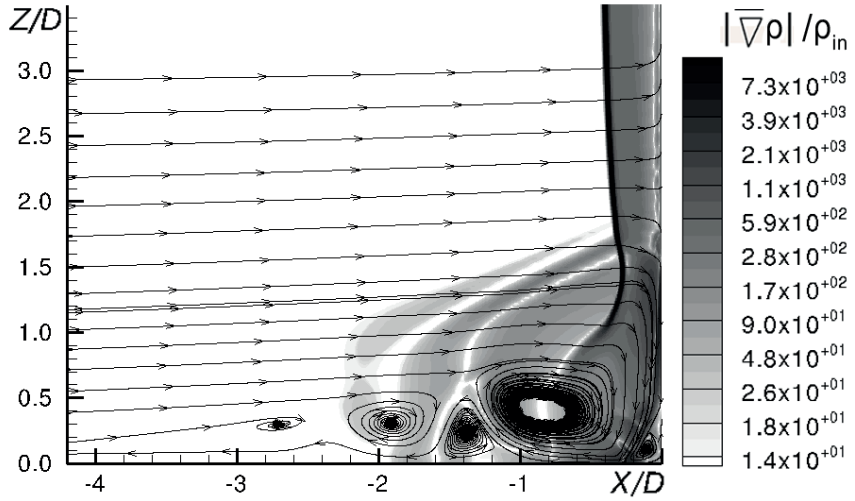

Fig. 5. Density gradient field and streamlines in symmetry plane. The figure shows values of the density gradient, computed by differentiation from dimensionless coordinates and corresponding to free-stream densities ρ_{in}

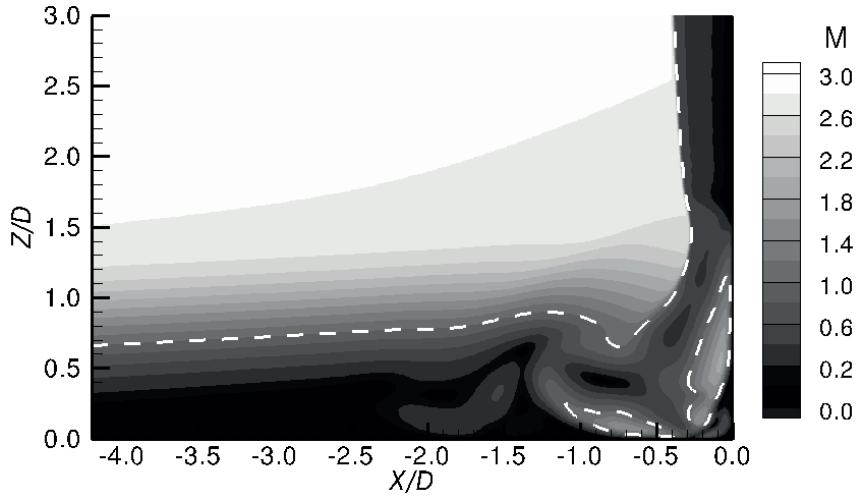

Fig. 6. Field of Mach number in symmetry plane; dashed line indicates sonic line M = 1

earlier in studies carried out for higher Mach and Reynolds numbers [15, 16]. A bow shock that occurs in front of the body interacts with the boundary layer, causing it to separate. The separation region induces oblique compression waves intersecting with the bow shock. Zones with supersonic velocities and local compression waves appear within the separation region, inducing secondary separation of the near-wall flow. As a result, an extended separation region with a chain of vortices evolves in front of the body, each of them becomes the "head" of a horseshoe-shaped vortex that surrounds the body.

The surface streamlines in Fig. 4 indicate the regions where the boundary layer separates and reattaches. The figure also shows the pressure distribution (related to the free-stream pressure value P_{in}). In particular, it can be seen that maximum pressure in the frontal part of the streamlined body exceeds the inlet pressure by about ten times.

More detailed visualization of the flow in the symmetry plane is given in Fig. 5, illustrating the

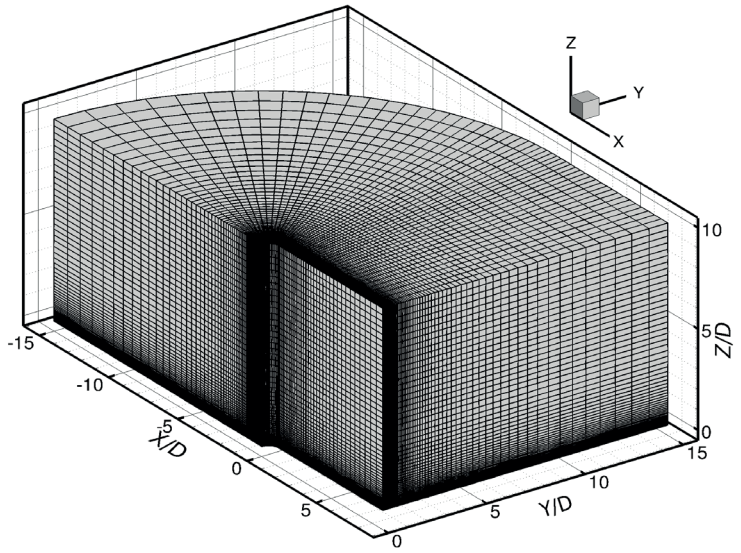

Fig. 7. Computational mesh 1, containing 0.3 million cells
(see the explanations in the text)

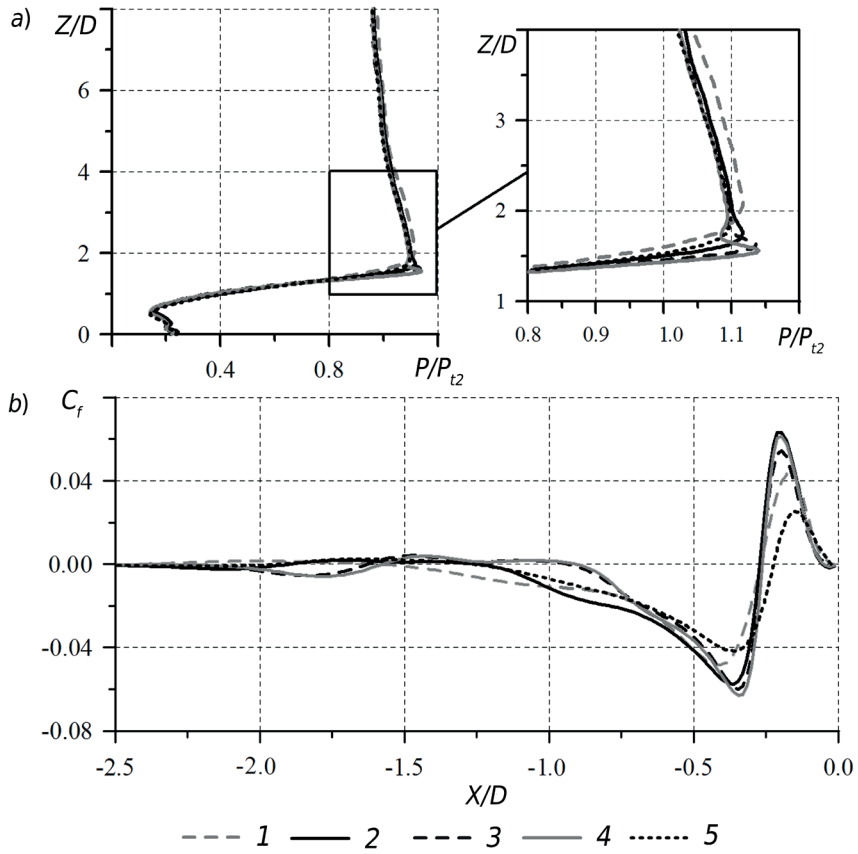

Fig. 8. Distributions of dimensionless pressure along frontal line (*a*)
and skin friction coefficient on plate along line of symmetry (*b*)
The figure shows computations by the AUSM scheme of second order of accuracy on meshes 1–4
(curve numbers coincide with mesh numbers) and first order of accuracy on mesh 4 (curve *5)*

shock wave structure with the density gradient field, combined with streamline patterns for the evolution of a vortex chain in the separation region. Analysis of the figure shows that the vortices filling the separation region induce oblique compression waves interacting with the bow shock. As a result of this interaction, the bow shock bends in the direction of the streamlined body, and a gas jet forms; as it flows onto the body, a zone of local pressure increasing arise. This effect is discussed in more detail below.

Fig. 6 shows the Mach number distribution in the symmetry plane; the dashed line indicates the sonic line (M = 1). While the flow is mainly subsonic in the separated separation region, two zones with supersonic flow are also observed. The flow moving from the stagnation region along the surface of the streamlined body towards the plate accelerates to supersonic speeds and then turns into a vortex, also reaching supersonic speed.

Mesh convergence. The study of mesh convergence was carried out using several quasi-structured meshes: mesh 1 contained 0.3 million cells, mesh 2 2.4 million cells, mesh 3 8.1 million cells and mesh 4 13.3 million cells. Mesh 2 was constructed by refining mesh 1 twice in each coordinate direction, mesh 3 by refining mesh 2 1.5 times, mesh 4 by refining mesh 3 only near the leading edge of the body (from 0 to 2.5 along the Z/D coordinate and from 2 to 0 along the X/D coordinate). All meshes had the same structure, with the mesh lines clustered to the streamlined body and to the surface of the plate. A general view of computational mesh 1 is shown in Fig. 7.

Fig. 8 shows the results obtained by the AUSM scheme using different meshes, including the pressure distribution along a front line on the surface of the body, and the distribution of the skin friction on the plate along a line of symmetry (the pressure was taken as the total pressure P_{t2} behind a normal shock wave, computed analytically). Notably, a characteristic increase in pressure was observed in the region at $Z/D \approx 1.5$, which is associated with a gas jet forming during the interaction of oblique compression waves with the bow shock. It is also interesting that the scheme with first-order accuracy does not reproduce this characteristic pressure peak even on the most refined mesh; this is primarily due to insufficient resolution of oblique compression waves. Moreover, a first-order scheme predicts a substantially simpler vortex structure of the separation region in front of the body.

The solution obtained on mesh 3 is very close to that obtained on mesh 4, both with respect to the pressure distribution and skin friction on the plate. This allows us to conclude that if schemes with second-order accuracy are used, mesh 4 is sufficiently refined for resolving all the details of the vortex structure near the junction between the body and the plate and also provides high-quality resolution of the shock-wave structure.

Comparison of solutions obtained by different schemes

Comparative computations were carried out on the most refined mesh (mesh 4) using the HLL and AUSM schemes of the first and second orders of accuracy. The most convenient way to compare the results obtained using different schemes is to analyze pressure distributions along selected lines on the streamlined body, as well as the predicted distributions of the skin friction along individual lines on the plate surface. The lines selected for analysis are shown in Fig. 9, and the distributions compared in Figs. 10 and 11.

Because schemes with first-order accuracy are highly dissipative, the solutions obtained by first-order and second-order schemes differ quite considerably in individual regions of the flow, both in the case of AUSM and in the case of the HLL scheme. Notably, however, the first-order AUSM scheme is fairly adequate in reproducing the shock-wave structure of the flow on the most refined mesh. Fig. 10 shows, in particular, that the pressure distribution over the body surface, obtained by the first-order AUSM scheme, is close to that computed by the second-order scheme (except for certain local regions); on the other hand, solution obtained with first-order HLL scheme strongly differs in the form.

Regarding the quality of viscous effects resolution of viscous effects, as noted above, the first-order AUSM scheme turns out to be too dissipative: using it results in a decreased number of resolved vortices that have reduced intensities even in case of the most refined mesh (see. Fig. 11). Using the first-order HLL scheme yields even less acceptable results: a completely different level of friction is predicted on a large part of the plate (see Fig. 11). While the results obtained by the AUSM and HLL schemes of the second order of accuracy are fairly close, there are also some local differences. In particular, it follows from analysis of the pressure

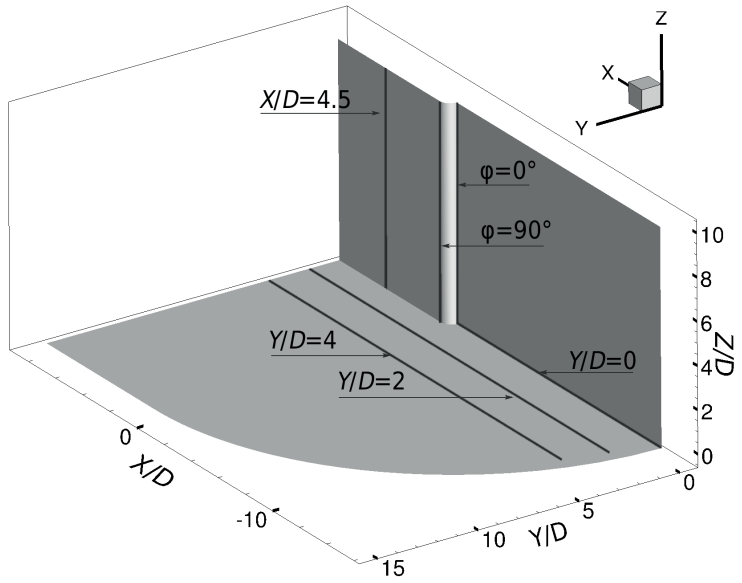

Fig. 9. Position of streamlines on body, selected for analysis of computed pressure and skin friction distributions
(see comparative analysis in Figs. 10, 11)

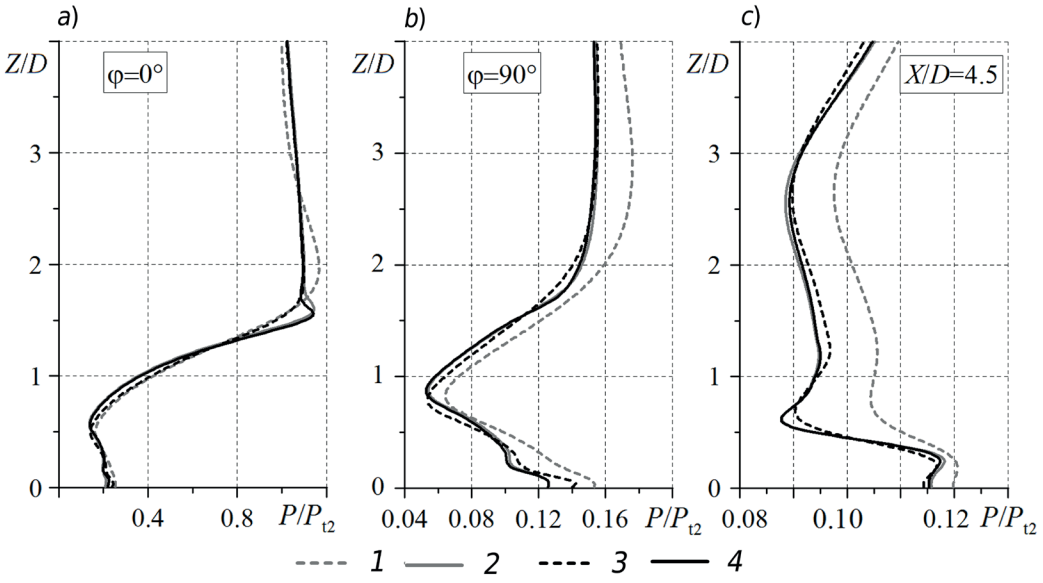

Fig. 10. Distributions of dimensionless pressure along vertical lines on surface of streamlined body (see Fig. 9): on frontal line (φ = 0°) (*a*), at the end of blunt part (φ = °90) (*b*), downstream (*X*/*D*) = 4.5 (*c*)
Computations were carried out by different schemes:
1, *2* correspond to HLL of first and second orders of accuracy, respectively;
3, *4* to AUSM of first and second orders of accuracy

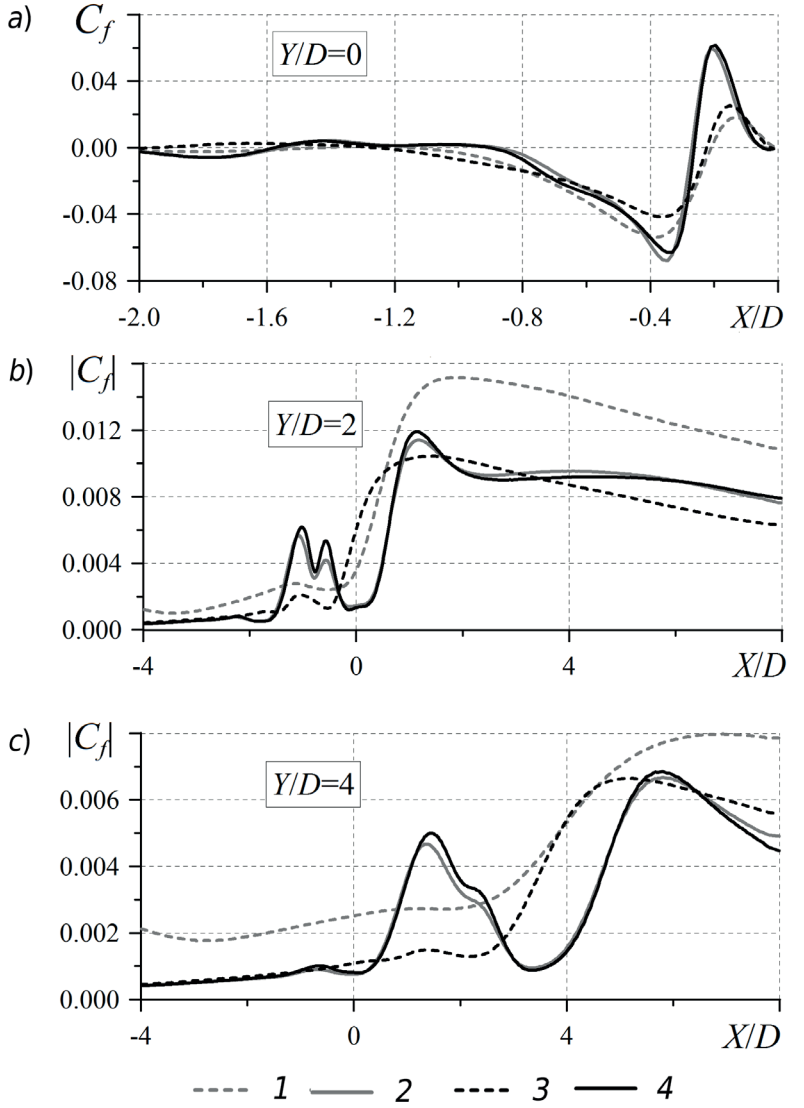

Fig. 11. Distributions of skin friction coefficient along several lines on plate surface: along line of symmetry (*a*) ($Y/D = 0$), at distances of two ($Y/D = 2$) and four ($Y/D = 4$) diameters from body, respectively (*b*, *c*).
Computations were carried out by different schemes:
1, *2* correspond to HLL of first and second orders of accuracy, respectively;
3, *4* to AUSM of first and second orders of accuracy

distribution along the front line (see Fig. 10) that the local pressure peak has a noticeably smaller width in the solution obtained by to the AUSM scheme. Conversely, analysis of the skin friction distribution on the plate (see Fig. 11) shows that the vortex intensity in the solution obtained by the HLL scheme is slightly lower than in the case of the AUSM scheme.

Conclusion

We have obtained a family of numerical solutions for a model problem of interaction of supersonic viscous gas (air) flow with an elongated blunt body mounted on a plate along which a laminar boundary layer evolves. Solutions using two schemes (HLL and AUSM) for convective flux evaluation on meshes of different sizes were obtained with a free-stream Mach number of 2.95 and a Reynolds number of 4000.

The flow evolving in the given configuration is three-dimensional, with clear effects of viscous-inviscid interaction. The separation region in front of the body has a complex vortex structure, with a family of horseshoe-shaped vortices that spread along the plate and expands around the body. Supersonic flow around the separation region induces oblique

compression waves; interacting with the bow shock, these waves generate a gas jet, which causes a local increase in pressure on the body.

According to the results of the mesh convergence study, we have found that if schemes with second order of accuracy are used, meshes containing 13–15 million hexagonal cells allow to resolve all the details of the vortex structure ~~of the flow~~ near the region where the body is connected to the plate, as well as to obtain high-quality resolution of the shock-wave structure. Schemes of the first-order of accuracy do not allow to reproduce significant characteristics of the flow caused by viscous effects even on the most detailed mesh among those used. The solutions obtained by the AUSM and HLL schemes of the second-order of accuracy are in good agreement, but on the whole, the HLL scheme proves to be more dissipative.

REFERENCES

1. **Dolling D.S.** Fifty years of shock-wave/boundary layer research? What next?, AIAA Journal. 39 (8) (2001) 1517–1531.

2. **Babinsky H., Harvey J.K.,** Shock wave/boundary-layer interactions, Cambridge University Press, Cambridge (2011).

3. **Devenport W.J., Simpson R.L.,** Time-dependent and time-averaged turbulence structure near the nose of a wing-body juncture, Journal of Fluid Mechanics. 210 (1990) 23–55.

4. **Fleming J.L., Simpson R.L., Cowling J.E., Devenport W.J.,** An experimental study of a turbulent wing-body junction and wake flow, Experiments in Fluids. 14 (5) (1993) 366–378.

5. **Ballio F., Franzetti S.,** Topological analysis of a junction vortex flow, Proceedings of Advances in Fluid Mechanics, Montreal, Canada, 24–26 May, 2000. WIT Press, Southampton (2000) 255–264.

6. **Levchenya A.M., Smirnov E.M., Goryachev V.D.,** RANS-based numerical simulation and visualization of the horseshoe vortex system in the leading edge endwall region of a symmetric body, International Journal of Heat and Fluid Flow. 31 (6) (2010) 1107–1112.

7. **Voytenko D.M., Zubkov A.I., Panov Yu.A.,** Obtekaniye tsilindricheskogo prepyatstviya na plastine sverkhzvukovym potokom gaza [Flow past a cylindrical obstacle on the plate by a supersonic gas stream], Fluid Dynamics. (1) (1966) 121.

8. **Aduyevskiy B.C., Medvedev K.I.,** Fizicheskiye osobennosti techeniya v oblasti otryva pri trekhmernom vzaimodeystvii pogranichnogo sloya s udarnoy volnoy [Physical features of the flow in the separation region in three-dimensional interaction of the boundary layer with a shock wave], Fluid Dynamics. (1) (1967) 25 –34.

9. **Teterin M.P.** Issledovaniye techeniya gaza v oblasti padeniya skachka uplotneniya na tsilindr, obtekayemyy potokom bolshoy sverkhzvukovoy skorosti [Investigation of gas flow in the region of the shock drop sealing on a cylinder, streamlined by a large supersonic flow], Fluid Dynamics. (2) (1967) 143–147.

10. **Dolling D.S., Bogdonoff S.M.,** Blunt fin-induced shock wave/turbulent boundary-layer interaction, AIAA Journal. 20 (12) (1982) 1674–1680.

11. **Ozcan O., Holt M.,** Supersonic separated flow past a cylindrical obstacle on a flat plate, AIAA Journal. 22 (5) (1984) 611–617.

12. **Houwing A.F.P., Smith D.R., Fox J.S., et al.,** Laminar boundary layer separation at a fin-body junction in a hypersonic flow, Shock Waves. 11 (1) (2001) 31–42.

13. **Borovoy V., Mosharov V., Radchenko V., Skuratov A.**, The shock-waves interference in the flow around a cylinder mounted on a blunted plate, 7th European Conference for Aeronautics and Space Sciences (EUCASS). Report 2017-63. (2017) 1 – 8.

14. **Hung C.-M., Buning P.G.,** Simulation of blunt-fin-induced shock-wave and turbulent boundary-layer interaction, Journal of Fluid Mechanics. 154 (1985) 163–185.

15. **Lakshmanan B., Tiwari S.N.,** Investigation of three-dimensional separation at wing/body junctions in supersonic flows, Journal of Aircraft. 31 (1) (1994) 64–71.

16. **Tutty O.R., Roberts G.T., Schuricht P.H.,** High-speed laminar flow past a fin-body junction, Journal of Fluid Mechanics. 737 (2013) 19–55.

17. **Peery K.M., Imlay S.T.,** Blunt body flow simulations, AIAA, Paper 88-2924 (1988).

18. **Quirk J.J.,** A contribution to the great Riemann solver debate, International Journal for Numerical Methods in Fluids. 18 (6) (1994) 555–574.

19. **Rodionov V.,** Artificial viscosity to cure the carbuncle phenomenon: The three-dimensional case, Journal of Computational Physics. 361 (2018) 50–55.

20. **Harten A., Lax P.D., van Leer B.,** On

upstream differencing and Godunov-type schemes for hyperbolic conservation laws, SIAM Review. 25 (1) (1983) 35–61.

21. **Liou M.S., Steffen C.J.,** A new flux splitting scheme, Journal of Computational Physics. 107 (1) (1993) 23–39.

22. **Toro E.F.,** Riemann solvers and numerical methods for fluid dynamics, Springer-Verlag, Berlin, Heidelberg (2009).

23. **Einfeldt B.,** On Godunov-type methods for gas dynamics, SIAM Journal on Numerical Analysis. 25 (2) (1988) 294–318.

24. **Roe P.L.,** Approximate Riemann solvers, parameter vectors, and difference schemes, Journal of Computational Physics. 43 (2) (1981) 357–372.

25. **Van Leer B.,** Towards the ultimate conservative difference scheme. V. A second order sequel to Godunov's method, Journal of Computational Physics. 32 (1) (1979) 101–136.

26. **Harten A.,** High resolution schemes for hyperbolic conservation laws, Journal of Computational Physics. 49 (3) (1983) 357–393.

27. **Le Touze S., Murrone A., Guillard H.,** Multislope MUSCL method for general unstructured meshes, Journal of Computational Physics. 284 (2015) 389–418.

28. **Bakhvalov P.A., Kozubskaya T.K.**, Skhema s kvaziodnomernoy rekonstruktsiyey peremennykh, opredelennykh v tsentrakh elementov trekhmernoy nestrukturirovannoy setki [Cell-centered quasi-one-dimensional reconstruction scheme on 3D hybrid meshes], Matem. modelirovaniye. 28 (3) (2016)79 –95.

29. **Van Albada G.D., Van Leer B., Roberts W.W.,** A comparative study of computational methods in cosmic gas dynamics, Astronomy and Astrophysics. 108 (1) (1982) 76–84.

Received 26.03.2019, accepted 03.04.2019.

THE AUTHORS

KOLESNIK Elizaveta V.
Peter the Great St. Petersburg Polytechnic University
29 Politechnicheskaya St., St. Petersburg, 195251, Russian Federation
kolesnik_ev@mail.ru

SMIRNOV Evgueni M.
Peter the Great St. Petersburg Polytechnic University
29 Politechnicheskaya St., St. Petersburg, 195251, Russian Federation
smirnov_em@spbstu.ru

SMIRNOVSKY Alexander A.
Peter the Great St. Petersburg Polytechnic University
29 Politechnicheskaya St., St. Petersburg, 195251, Russian Federation
smirta@mail.ru

СПИСОК ЛИТЕРАТУРЫ

1. **Dolling D.S.** Fifty 2019s of shock-wave/ boundary layer research? What next? // AIAA Journal. 2001. Vol. 39. No. 8. Pp. 1517–1531.

2. **Babinsky H., Harvey J.K.** Shock wave/ boundary-layer interactions. Cambridge: Cambridge University Press, 2011. 461 p.

3. **Devenport W.J., Simpson R.L.** Time-dependent and time-averaged turbulence structure near the nose of a wing-body juncture // Journal of Fluid Mechanics. 1990. Vol. 210. Pp. 23–55.

4. **Fleming J.L., Simpson R.L., Cowling J.E., Devenport W.J.** An experimental study of a turbulent wing-body junction and wake flow // Experiments in Fluids. 1993. Vol. 14. No. 5. Pp. 366–378.

5. **Ballio F., Franzetti S.** Topological analysis of a junction vortex flow // Proceedings of Advances in Fluid Mechanics. Montreal, Canada. 2000. 24–26 May. WIT Press, Southampton. 2000. Pp. 255–264.

6. **Levchenya A.M., Smirnov E.M., Goryachev V.D.** RANS-based numerical simulation and visualization of the horseshoe vortex system in the leading edge endwall region of a symmetric body // International Journal of Heat and Fluid Flow. 2010. Vol. 31. No. 6. Pp. 1107–1112.

7. **Войтенко Д.М., Зубков А.И., Панов Ю.А.** Обтекание цилиндрического препятствия на пластине сверхзвуковым потоком газа //

Известия АН СССР. Механика жидкости и газа. 1 № .1966. С. 121.

8. **Адуевский В.С., Медведев К.И.** Физические особенности течения в области отрыва при трехмерном взаимодействии пограничного слоя с ударной волной // Известия АН СССР. Механика жидкости и газа. 1 № .1967. С. 25–34.

9. **Тетерин М.П.** Исследование течения газа в области падения скачка уплотнения на цилиндр, обтекаемый потоком большой сверхзвуковой скорости // Известия АН СССР. Механика жидкости и газа. 1967. № 2. С. 143 –147.

10. **Dolling D.S., Bogdonoff S.M.** Blunt fin-induced shock wave/turbulent boundary-layer interaction // AIAA Journal. 1982. Vol. 20. No. 12. Pp. 1674–1680.

11. **Ozcan O., Holt M.** Supersonic separated flow past a cylindrical obstacle on a flat plate // AIAA Journal. 1984. Vol. 22. No. 5. Pp. 611–617.

12. **Houwing A.F.P., Smith D.R., Fox J.S., Danehy D.M., Mudford N.R.** Laminar boundary layer separation at a fin-body junction in a hypersonic flow // Shock Waves. 2001. Vol. 11. No. 1. Pp. 31–42.

13. **Borovoy V., Mosharov V., Radchenko V., Skuratov A.** The shock-waves interference in the flow around a cylinder mounted on a blunted plate //7th European Conference for Aeronautics and Space Sciences (EUCASS). 2017. Report 2017-63. Pp. 1 – 8.

14. **Hung C.-M., Buning P.G.** Simulation of blunt-fin-induced shock-wave and turbulent boundary-layer interaction // Journal of Fluid Mechanics. 1985. Vol. 154. Pp. 163–185.

15. **Lakshmanan B., Tiwari S.N.** Investigation of three-dimensional separation at wing/body junctions in supersonic flows // Journal of Aircraft. 1994. Vol. 31. No. 1. Pp. 64–71.

16. **Tutty O.R., Roberts G.T., Schuricht P.H.** High-speed laminar flow past a fin–body junction // Journal of Fluid Mechanics. 2013. Vol. 737. Pp. 19–55.

17. **Peery K.M., Imlay S.T.** Blunt body flow simulations // AIAA. 1988. July. Paper 88-2924.

18. **Quirk J.J.** A contribution to the great Riemann solver debate // International Journal for Numerical Methods in Fluids. 1994. Vol. 18. No. 6. Pp. 555–574.

19. **Rodionov V.** Artificial viscosity to cure the carbuncle phenomenon: The three-dimensional case // Journal of Computational Physics. 2018. Vol. 361. Pp. 50–55.

20. **Harten A., Lax P.D., van Leer B.** On upstream differencing and Godunov-type schemes for hyperbolic conservation laws // SIAM Review. 1983. Vol. 25. No. 1. Pp. 35–61.

21**. Liou M.S., Steffen C.J.** A new flux splitting scheme // Journal of Computational Physics. 1993. Vol. 107. No. 1. Pp. 23–39.

22. **Toro E.F.** Riemann solvers and numerical methods for fluid dynamics. Berlin, Heidelberg: Springer-Verlag, 2009. 724 p.

23. **Einfeldt B.** On Godunov-type methods for gas dynamics // SIAM Journal on Numerical Analysis. 1988. Vol. 25. No. 2. Pp. 294–318.

24. **Roe P.L.** Approximate Riemann solvers, parameter vectors, and difference schemes // Journal of Computational Physics. 1981. Vol. 43. No. 2. Pp. 357–372.

25. **Van Leer B.** Towards the ultimate conservative difference scheme. V. A second order sequel to Godunov's method // Journal of Computational Physics. 1979. Vol. 32. No. 1. Pp. 101–136.

26. **Harten A.** High resolution schemes for hyperbolic conservation laws // Journal of Computational Physics. 1983. Vol. 49. No. 3. Pp. 357–393.

27. **Le Touze** C., **Murrone A., Guillard H.** Multislope MUSCL method for general unstructured meshes // Journal of Computational Physics. 2015. Vol. 284. Pp. 389–418.

28. Бахвалов П.А., Козубская **Т.К.** Схема с квазиодномерной реконструкцией переменных, определенных в центрах элементов трехмерной неструктурированной сетки // Математическое моделирование. 2016. Т. 28. № 3. С. 79–95.

29. **Van Albada G.D., Van Leer B., Roberts W.W.** A comparative study of computational methods in cosmic gas dynamics // Astronomy and Astrophysics. 1982. Vol. 108. No. 1. Pp. 76–84.

Статья поступила в редакцию 26.03.2019, принята к публикации 03.04.2019.

СВЕДЕНИЯ ОБ АВТОРАХ

КОЛЕСНИК Елизавета Владимировна – инженер кафедры «Гидроаэродинамика, *горение и теплообмен» Санкт-Петербургского политехнического университета Петра Великого.*
195251, Российская Федерация, г. Санкт-Петербург, Политехническая ул., 29
kolesnik_ev@mail.ru

СМИРНОВ Евгений Михайлович – доктор физико-математических наук, заведующий кафедрой «Гидроаэродинамика, *горение и теплообмен» Санкт-Петербургского политехнического университета Петра Великого.*
195251, Российская Федерация, г. Санкт-Петербург, Политехническая ул., 29
smirnov_em@spbstu.ru

СМИРНОВСКИЙ Александр Андреевич – кандидат физико-математических наук, доцент кафедры «Гидроаэродинамика, *горение и теплообмен» Санкт-Петербургского политехнического университета Петра Великого.*
195251, Российская Федерация, г. Санкт-Петербург, Политехническая ул., 29
smirta@mail.ru

© Peter the Great St. Petersburg Polytechnic University, 2019